The Journal of Chemical Physics

RESEARCH ARTICLE | MARCH 15 2019

Ultrafast photodissociation dynamics and nonadiabatic coupling between excited electronic states of methanol probed by time-resolved photoelectron spectroscopy

Elio G. Champenois; Loren Greenman; Niranjan Shivaram ; James P. Cryan; Kirk A. Larsen; Thomas N. Rescigno; C. William McCurdy ; Ali Belkacem; Daniel S. Slaughter

J. Chem. Phys. 150, 114301 (2019)
https://doi.org/10.1063/1.5079549

AIP Publishing

The Journal of Chemical Physics ARTICLE scitation.org/journal/jcp

Ultrafast photodissociation dynamics and nonadiabatic coupling between excited electronic states of methanol probed by time-resolved photoelectron spectroscopy

Cite as: J. Chem. Phys. 150, 114301 (2019); doi: 10.1063/1.5079549
Submitted: 31 October 2018 • Accepted: 26 February 2019 •
Published Online: 15 March 2019

Elio G. Champenois,[1,2] Loren Greenman,[1,3,4] Niranjan Shivaram,[1,5] James P. Cryan,[6] Kirk A. Larsen,[1,2] Thomas N. Rescigno,[1] C. William McCurdy,[1,3] Ali Belkacem,[1] and Daniel S. Slaughter[1,a)]

AFFILIATIONS

[1]Chemical Sciences Division, Lawrence Berkeley National Laboratory, Berkeley, California 94720, USA
[2]Graduate Group in Applied Science and Technology, University of California, Berkeley, California 94720, USA
[3]Department of Chemistry, University of California, Davis, California 95616, USA
[4]Department of Physics, Kansas State University, Manhattan, Kansas 66506, USA
[5]Linac Coherent Light Source, SLAC National Accelerator Laboratory, Menlo Park, California 94025, USA
[6]Stanford PULSE Institute, SLAC National Accelerator Laboratory, Menlo Park, California 94025, USA

[a)]DSSlaughter@lbl.gov

ABSTRACT

The electronic and nuclear dynamics in methanol, following 156 nm photoexcitation, are investigated by combining a detailed analysis of time-resolved photoelectron spectroscopy experiments with electronic structure calculations. The photoexcitation pump pulse is followed by a delayed 260 nm photoionization probe pulse to produce photoelectrons that are analyzed by velocity map imaging. The yields of mass-resolved ions, measured with similar experimental conditions, are found to exhibit the same time-dependence as specific photoelectron spectral features. Energy-resolved signal onset and decay times are extracted from the measured photoelectron spectra to achieve high temporal resolution, beyond the 20 fs pump and probe pulse durations. When combined with *ab initio* calculations of selected cuts through the excited state potential energy surfaces, this information allows the dynamics of the transient excited molecule, which exhibits multiple nuclear and electronic degrees of freedom, to be tracked on its intrinsic few-femtosecond time scale. Within 15 fs of photoexcitation, we observe nuclear motion on the initially bound photoexcited $2^1A''$ (S_2) electronic state, through a conical intersection with the $1^1A'$ (S_3) state, which reveals paths to photodissociation following C–O stretch and C–O–H angle opening.

I. INTRODUCTION

Molecules excited by light can evolve by coupled nuclear and electronic motion over ultrafast time scales.[1] In many photochemical reactions, the products and their relative yields depend sensitively on the details of these coupled molecular dynamics and processes that occur within a few femtoseconds.[2–7] For example, near a conical intersection, where the evolving molecular geometry finds two or more electronic states of equal potential energy, nonadiabatic transitions can occur, enabling important non-radiative relaxation mechanisms, such as competing isomerization or dissociation pathways.[8,9] Considerable interest in investigating such dynamics on their natural femtosecond time scales has driven recent developments of time-resolved spectroscopic methods employing few-cycle infrared lasers and broadband attosecond pulses.[10–13]

Time-resolved photoelectron spectroscopy (TRPES) has arguably become the gold standard to study ultrafast nonadiabatic dynamics in neutral excited molecules.[14–16] A measurement of the instantaneous photoelectron binding energy of the excited wavepacket can be parsed into contributions from each state involved in the electronic relaxation process,[17,18] allowing kinetic models to be constructed. Photoelectron spectra are also

sensitive to excited vibrational wavepacket dynamics due to the dependence of the binding energy on the evolving molecular geometry.[19–21] Signatures of such dynamics have been observed in TRPES as shifts[7,19,22–27] in the measured photoelectron kinetic energy as the probe pulse delay is increased. Such shifts are a direct result of the wavepacket motion on the excited state potential energy surface (PES), due to the configuration-dependent ionization potential.

We temporally and spectrally resolve photodissociation dynamics of methanol following excitation to the $2^1A''$ (S_2) electronic state at 156 nm, using TRPES to identify and follow the photochemical reaction. Using a 260 nm single-photon probe, we measure dynamical features in the photoelectron spectra as a function of the pump-probe time delay and quantify them to extract signatures of the nuclear motion that emerges in the first few femtoseconds following excitation. Measurements of the photoelectron kinetic energy E_{e^-} allow the determination of the transient binding energy $\mathcal{E}(\vec{\mathbf{R}})$ of the system for the known probe photon energy $\hbar\omega_{probe}$

$$\begin{aligned}\mathcal{E}(\vec{\mathbf{R}}) &= \hbar\omega_{probe} - E_{e^-} \\ &= E_c(\vec{\mathbf{R}}) - E_n(\vec{\mathbf{R}}),\end{aligned} \tag{1}$$

where the potential energies of the cation $E_c(\vec{\mathbf{R}})$ and the neutral excited state $E_n(\vec{\mathbf{R}})$ depend on the nuclear coordinates $\vec{\mathbf{R}}$. When interpreted with the aid of electronic structure calculations, which assist in reducing the dimensionality of the dynamics through the identification of a characteristic reaction coordinate, this technique enables the nuclear wavepacket to be tracked as it evolves on the PES.

Methanol plays an important role in atmospheric chemistry, fuels, and energy transport,[28–30] and the excited state dynamics of methanol are relevant to each of these applications. Direct investigation of excited state dynamics of methanol in the time domain has been challenging due to the high electronic excitation energies, the ultrafast nuclear motion on the excited states, and the relative complexity of the molecule involving two fundamental functional groups. In previous studies, several neutral dissociation channels were observed following photoexcitation of the $2^1A''$ (S_2) state in methanol.[31–33] Among these, the dominant two-body breakup processes produce either $CH_3O + H$ or $CH_3 + OH$, while $CH_2OH + H$ and $CH_2O + H_2$ are also produced with lower yields. The S_2 excited state is bound along the O–H and C–O coordinates, while the $1^1A''$ (S_1) state is dissociative in the same coordinates.[34] Previous calculations revealed avoided crossings between the S_1 and S_2 states along each of these coordinates,[34] which suggested that the observed dissociation occurs after a nonadiabatic transition to the lower of these two $^1A''$ states.[32,33] Analysis of the fragment kinetic energy distributions for the O–H and C–O dissociation channels revealed that most of the available energy is channeled into translational kinetic energy, which also supports the possible mechanism of prompt dissociation on the S_1 PES, which connects asymptotically to the $CH_3O + H$ and $CH_3 + OH$ thermodynamic limits.[32,33,35–37]

In the valence isoelectronic system CH_3SH, the S_1 and S_2 surfaces were previously explored by neutral fragment velocity map imaging[38] and *ab initio* theory.[8,39,40] In CH_3SH, a conical intersection between the S_2 and S_1 PESs, involving C–S bond stretch and S–H motion, enables dissociation. In the present investigation, we explore the possibility of an analogous conical intersection between the S_2 and S_1 PESs in methanol and address whether the nuclear dynamics following excitation to the S_2 state are mediated by S_1, or a previously ignored $1^1A'$ (S_3) state.

II. METHODS

A. Experimental details

The experimental setup is described in detail elsewhere;[26,41] therefore, only a brief overview is provided here. A 25 mJ, 25 fs, 1 kHz Ti:sapphire near-infrared (NIR) laser system generates vacuum and extreme ultraviolet light via the non-linear process of high-order harmonic generation. The pump and probe pulses are generated by focusing (6 m, f/200) the 780 nm NIR pulses in a 25 Torr argon gas cell, 10 cm in length, to generate odd harmonics. The fundamental NIR component is then suppressed by $>10^6$ by transmission through a pair of near-grazing incidence dichroic mirrors that have high reflectivity in the vacuum and extreme ultraviolet. The odd harmonics are split into two parallel beams by D-shaped filters and a split mirror interferometer in a back-focusing geometry. In the present experiments, the filters and mirror coatings isolate the fifth harmonic (156 nm, 7.95 eV) of the fundamental for the pump arm and the third harmonic (260 nm, 4.77 eV) for the delayed probe arm.

The pulse energy partitioning between the pump and probe beams at the interferometer was optimized to maximize the relative ionization rate when the pump-probe beams are coincident, compared to the rate when the probe arrived 50 fs–150 fs earlier than the pump, and to avoid nonlinear conditions. The foci of the two beams were spatially overlapped in a velocity map imaging spectrometer, which allowed the kinetic energy spectra of either the electrons or ions, resulting from the photoionization of target molecules, to be recorded. A set of microchannel plates, a phosphor screen, and a CCD camera captured the projected electron or ion momentum distributions, and the pBASEX algorithm[42] was used to recover the kinetic energy distributions. For ions, a fast voltage pulse applied to the detector at specific times relative to the ionizing laser pulse allowed different ion fragments to be isolated by their mass-to-charge ratio. The global instrument response function was measured to have a Gaussian width of 31.2 fs ± 0.9 fs (full width at half maximum) in the time-dependent ion yield for non-resonant two-photon ionization of xenon. Methanol vapor, from a container held at room temperature, was controlled through a variable leak valve to produce an effusive molecular beam from a long 100 μm-diameter capillary, with the capillary exit being 4 cm from the pump and probe foci.

Each photoelectron spectrum consisted of 50 frames, with each frame capturing photoelectrons accumulated from 27 laser pulses. The photoelectron spectra were measured for each pump-probe delay 175 times in a randomized order to minimize artifacts due to small drifts in the laser intensity and target gas pressure. These separate measurements were used to estimate the variance in the signal at each camera pixel for each pump-probe delay. The off-diagonal elements of the resultant covariance matrix were set to zero. These errors were propagated through the background subtraction and pBASEX fit to find the covariance matrix for the time- and energy-dependent photoelectron signal

I($\mathcal{E}$, t). This approach allowed uncertainties in the signal in each energy-time delay bin to be propagated throughout the following analysis.

B. Theoretical calculations

We used equation-of-motion coupled-cluster theory with single and double excitations (EOM-CCSD)[43,44] and an aug-cc-pVTZ basis set[45] to calculate the PES of the ground and first few excited states of neutral methanol. The ground state of the cation was calculated using spin-restricted open-shell coupled cluster theory (RHF-RCCSD/aug-cc-pVTZ).[46,47] Since methanol's excited states have significant Rydberg character, it is necessary to use augmented functions in the basis set. At geometries with stretched methanol bonds, we used unrestricted reference functions (UHF-EOM-CCSD)[48–52] to ensure that the EOM-CCSD results were reliable and the presence of multireference correlation did not significantly change the results. The EOM-CCSD calculations were performed using the MOLPRO electronic structure suite,[53,54] while those with an unrestricted reference were performed using the NWChem package.[48,49] Conical intersections were discovered using gradient-based searches as implemented in MOLPRO and by minimizing the energy difference between the two states of interest using a Nelder-Mead simplex method.[55]

Calculations of the two-dimensional potentials in Fig. 5 were performed by optimizing the energy on the cation surface with respect to the other internal coordinates. The dimensions C–O–H angle and C–H bond length were chosen partially by comparison to Buenker *et al.*[34] Additional degrees of freedom were considered, and these two dimensions were chosen to be the most relevant (see the supplementary material for details). The geometry optimizations used multireference Rayleigh-Schrödinger perturbation theory,[56–59] using an active space of 3 electrons in 5 orbitals. Loose geometry convergence parameters were used for some of the geometries far from equilibrium. A single-point energy calculation at the EOM-CCSD and RHF-RCCSD levels for the neutral molecule and cation, respectively, was performed on the optimized geometries.

III. RESULTS AND DISCUSSION

A. Signal onset times and resolving a fast dissociative reaction pathway

The experimental time-resolved photoelectron spectra, for excitation at 156 nm and ionization by a delayed 260 nm probe pulse, are shown in Fig. 1. The overall photoelectron yield decays within ~200 fs. We observe features in the photoelectron spectra that shift as the time delay is increased, with a peak first appearing near the binding energy of 2.9 eV, which is also the difference between the vertical ionization potential[60] and the pump photon energy of 7.95 eV and corresponds to a photoelectron kinetic energy of 1.87 eV in the present experiments. This peak extends towards higher binding energies (lower kinetic energies) with longer time delays. The probe pulse intensity and photon energy are carefully selected to prevent the population of excited electronic states of the cation so that the TRPES features are due to ultrafast wavepacket motion on the neutral excited states and the topology of the ground state PES of the cation. The photoelectron angular

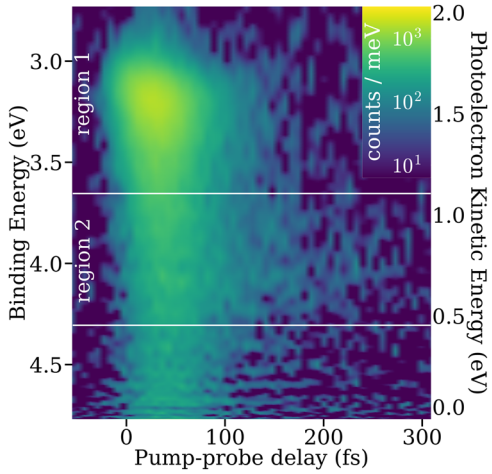

FIG. 1. Time-resolved photoelectron spectra from ionization at 260 nm following excitation at 156 nm, taken in 6.57 fs steps. The background, due to multiphoton ionization from the pump or probe alone, is removed by subtracting the averaged spectra for the probe pulse arriving earlier than the pump pulse within a time window of t = −50 fs to t = −150 fs. For positive time delays, the probe pulse arrives after the pump pulse. White lines partition the spectra into regions that are discussed in the text.

distributions were measured and determined to not change significantly with the pump-probe time delay, so they are not discussed further here.

To quantify the measured photoelectron spectra, we use a global fitting algorithm that fits each energy-slice, $I(\mathcal{E}, t)$, with a function parameterized by the energy-dependent signal onset time $t_0(\mathcal{E})$ and exponential decay time $\tau(\mathcal{E})$, convolved with a global Gaussian function g of width σ

$$I(\mathcal{E},t) = A(\mathcal{E})\left[H(t-t_0(\mathcal{E})) \times \exp\left(-\frac{t-t_0(\mathcal{E})}{\tau(\mathcal{E})}\right)\right] \otimes g(t);\sigma\Big), \quad (2)$$

where H(t) is the Heaviside step function[26] and the global fit parameter sigma was found to be σ = 44.8 ± 0.5 fs. The global Gaussian convolution models the instrument response function and the energy width of the photoelectron signal that could be expected as the nuclear wavepacket explores the excited state PES; however, the latter is independent of binding energy. The advantage of this simple approach is that the fitting procedure is both well-constrained and precise. The retrieved signal onset times, $t_0(\mathcal{E})$, and signal decay times, $\tau(\mathcal{E})$, are shown in Fig. 2. Equation (2) provides an energy-dependent framework to the TRPES technique to allow access to time-resolved dynamics within the duration of pump and probe pulses. This framework is well-adapted to describing the dynamics of a nuclear wavepacket evolving on excited states without requiring one or more specific transition states and their associated reaction kinetics to be defined. Further details, including a comparison between this approach and a fit using decay associated spectra,[61] can be found in the supplementary material.

The retrieved onset times of Fig. 2 can be interpreted as the time it takes for the wavepacket to arrive at a region of the PES with a specified binding energy. Following photoexcitation, the

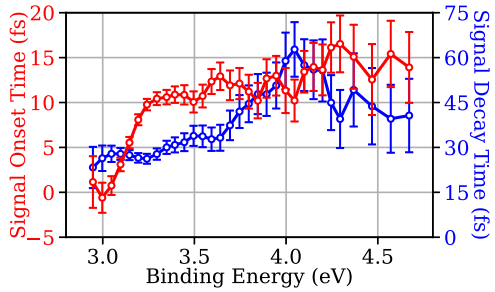

FIG. 2. Retrieved photoelectron signal onset times $t_0(\mathcal{E})$ (red) and decay times $\tau(\mathcal{E})$ (blue) for various binding energy slices extracted from the data of Fig. 1, with the error bars representing one standard deviation in the uncertainty of the fit parameters. The slices are 50 meV wide, except above 4.3 eV, where each slice is 100 meV wide.

excited state wavepacket rapidly moves away from Franck-Condon geometries to a region of increased binding energy. Over the first ~10 fs, the binding energy increases smoothly at 0.025 eV/fs. Above 3.3 eV, there is an abrupt change in this rate to a slower monotonic increase of about 0.3 eV/fs, which continues for the remainder of the measurable binding energies up to 4.77 eV, suggesting neutral dissociation. As the binding energy increases, the dissociating wavepacket could be expected to sample a larger volume of the excited state PESs. Such spreading of the nuclear wavepacket may also contribute to the change in the rate of the signal onset time with binding energy. Thus, by analyzing the time-dependence of the excited state binding energies (see onset times in Fig. 2), the initial motion of the excited molecule can be accessed on time scales significantly shorter than the ~20 fs widths of the pump and probe pulses.

In methanol, there are 12 internal degrees of freedom. While this number is small relative to other alcohols, examining excited state dynamics in methanol is challenging due to the high dimensionality of its PESs. In the present work, we use equation-of-motion coupled-cluster theory to examine cuts of the PESs of the involved excited states. We define a 1-dimensional coordinate, using the following procedure, to significantly reduce the dimensionality of the system.

A comparison can be made between the experiment and theory by considering the measured binding energies. The experiment measures the signal onset times as a function of the binding energy $t_0(\mathcal{E})$, while the theory predicts the binding energies for an electronic state as a function of nuclear geometry $\mathcal{E}(\vec{\mathbf{R}})$, i.e., the PES. By defining a one-dimensional reaction coordinate, using its potential energy curve and the experimental binding energy $\mathcal{E}(t)$, we can approximate $\vec{\mathbf{R}}(t)$ by inverting these curves. While there are many such coordinates that can lead to the same $\mathcal{E}(t)$, our knowledge of the multidimensional PES and the experimental results suggest that this particular choice of coordinate gives a good approximation to $\vec{\mathbf{R}}(t)$.

Both the C–O stretch and the C–O–H bond angle were considered, following the measured rates for methanol and the deuterated species presented in Sec. III B, and the earlier study of Buenker *et al.*[34] To explain the measured photoelectron spectral shifts, several trial reaction coordinates involving simultaneous stretching of the C–O bond and the opening of the C–O–H bond angle were considered by taking different cuts from the calculated two-dimensional surfaces. The selected example, representative of the global topology of S_2, is presented in Fig. 3. This reaction coordinate was selected following an inspection of the two-dimensional surface to capture the relevant processes in a concise illustration. The initial excited wavepacket will advance on the S_2 ($2^1A''$) PES along this coordinate until it reaches a region of nonadiabatic coupling between this surface and that of S_3 ($1^1A'$). At and in the neighborhood of this geometry, internal conversion to S_3 becomes possible. Starting at this geometry on S_3, the same fragments, specifically those due to C–O and O–H cleavage, can be reached as previously considered.[32,33] The S_3 and S_1 ($1^1A''$) surfaces become degenerate at linear C–O–H geometries; however, crossing to S_1 is not required for dissociation, in contrast to the valence isoelectronic system CH_3SH, and previous assumptions about methanol.

The calculations along this reaction coordinate agree well with the features of the signal onset time measurement. At 3.3 eV, the abrupt change in the gradient of the measured binding energy-dependent onset time (Fig. 2) is consistent with a transition from

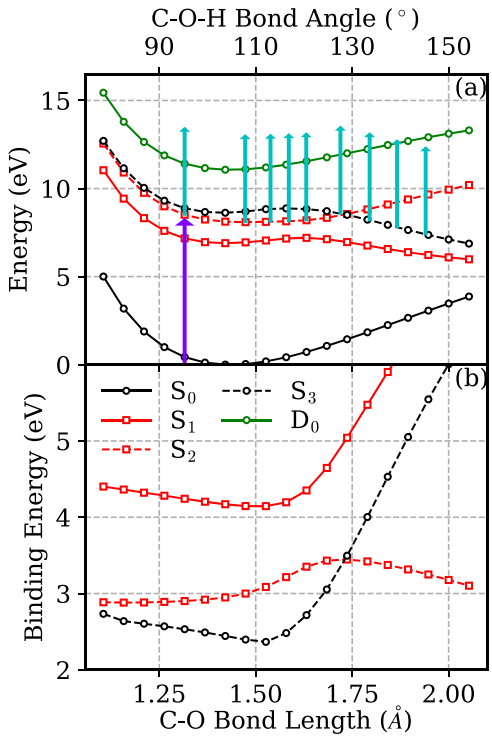

FIG. 3. Calculated cuts (a) of the potential energy surfaces and (b) the associated photoelectron binding energies for the first two A′ states (black lines, S_0 and S_3), the first two A″ states (red lines, S_1 and S_2), and the cation ground state (green line, D_0) as the C–O bond distance (lower axis) and the C–O–H bond angle (upper axis) are simultaneously stretched and opened, with the arrows indicating the initial excitation (magenta) and time-delayed ionization (cyan). The ionization is shown in 2 fs steps starting at pump-probe overlap, using the experimental binding energy dependent onset times of Fig. 2 and the binding energy calculations shown here, and making the approximation that all of the measured binding energy shifts are due to motion along this coordinate.

the initially excited S_2 to S_3, where the binding energy depends more strongly on the nuclear geometry. The energetic location of this transition is also in good agreement with the calculated crossing geometry of these two states at a binding energy of 3.45 eV, as shown in Fig. 3. After the internal conversion to the dissociative state, the other coordinates begin to play a role. Notably, the O–H bond breaking on S_3 is expected to have a steep gradient compared to the other dissociation channels.[62]

The measured signal decay times of Fig. 2 characterize the time scale for the excited state wavepacket to exit a region of the PES at a specified binding energy. For binding energies associated with S_2, the decay times are between 25 and 30 fs, revealing the time needed to completely depopulate the Franck-Condon region.

The previous studies of this excited state of methanol consider only the crossing between the two A″ states S_1 and S_2.[32,34] A calculation on CH_3SH[40] suggests that an analogous conical intersection could be arrived at largely through C–S (analogous to C–O) bond stretch. We performed a search for a conical intersection between S_1 and S_2 in methanol and only found one in a region of the PES that is energetically inaccessible for the present experiments. The importance of the A′ state S_3 in the dissociation of methanol underlines the weak correspondence in the excited state dynamics of the two isoelectronic molecules. The previously ignored S_3 state appears to be responsible for the rapid relaxation within 15 fs observed in the present experiments and is also consistent with previous measurements.[32,34]

B. Correlating delayed-onset photoelectrons with hydrogen elimination

Excited methanol fragments through multiple dissociation channels following photoexcitation. Both the CH_2OH^+ + H channel and the CH_2O^+ + H_2 channel, with appearance energies of 11.7 eV and 12.3 eV, respectively,[63] are energetically accessible for the photon energies of the present experiments. We measured the time-dependent ion yields for the species associated with these H and H_2 elimination channels along with the bound ionic methanol channel using the same experimental apparatus and the same 156 nm pump, 260 nm probe scheme. The results are shown in Fig. 4. The fragment ion kinetic energy distribution was too small to resolve any anisotropy; therefore, the kinetic energy and anisotropy are not discussed here. A fast rise in the CH_3OH^+ yield near t_0 with a fast decay and a slightly delayed rise in the CH_2OH^+ yield with a slower decay are observed. Hydrogen loss in the latter channel was confirmed to occur exclusively from the methyl site of methanol by performing the same experiment with its deuterated isotopologues CD_3OH and CH_3OD. Only the parent ion CH_3OH^+ and the fragment ion CH_2OH^+ were found to exhibit time dependence in their ion yields. There was no significant time-dependent yield of CH_2O^+.

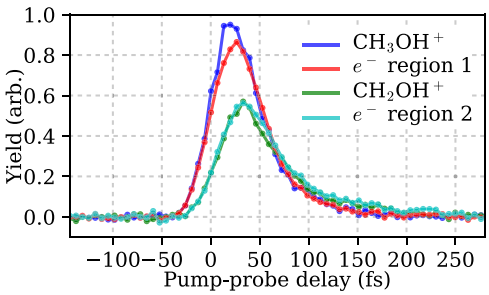

FIG. 4. Pump-probe time-dependent yield of the two ion and photoelectron channels. In this analysis, only the total ion and photoelectron yields were normalized. The two electron regions correspond to binding energies of 2.9–3.65 eV (red, fast decay) and 3.65–4.3 eV (cyan, slow decay), as labeled in Fig. 1.

Fitting the time-dependent ion yields with the ansatz of Eq. (2) gives a 7 fs delay for the fragment signal relative to that of the parent ion and a 30 fs and 45 fs 1/*e* lifetime for the parent and fragmented ion, respectively. Although these ion yield measurements were not made in coincidence with the photoelectron measurements, the faster CH_3OH^+ yield correlates well with that of photoelectrons with binding energies between the ionization potential and 11.6 eV (region 1 in Fig. 1), as shown in Fig. 4, and the slower CH_2OH^+ yield correlates with that of binding energies between 3.65 eV and 4.3 eV (region 2 in Fig. 1), where the signal takes longer to decay (Fig. 2). Note that the time-dependence in the fragment ion yield and the correlated photoelectron yield exhibits later onset times followed by longer decay times. The fitted signal decay lifetimes for the fragment and parent ion yields, along with the corresponding photoelectron yields from each of the binding energy bands described above, are summarized in Table I for each target species. Although C–H dissociation occurs on the methyl site of the molecule, the signal decay time scales were greatly affected by hydroxyl deuteration and less so by fully deuterating the methyl functional group, indicating that hydroxyl motion in the excited state plays an important role in facilitating the methyl hydrogen elimination. A previous experimental study of 157 nm photodissociation[32] determined two-body methyl hydrogen elimination to be a minor photodissociation channel (3% compared to two-body O–H break); therefore, significant C–H break is not expected to occur on the neutral excited states, but may occur on the ground state of the cation. Deuteration did not strongly affect the appearance time of the fragment ion, relative to the parent ion, or the photoelectron signal onset times, indicating that stretching of the C–O bond, rather than hydrogen motion, limits the rate of the initial dynamics.

To gain insight into the dynamics leading to methyl hydrogen loss in the present experiments, we turn to the computed 2-dimensional cuts, along the C–H stretch and the C–O–H angle coordinates, of the S_2 and S_3 excited states and the cation ground state D_0, which are shown in Fig. 5. The cuts were chosen following

TABLE I. Fitted exponential decay times, in femtoseconds, of the ion and electron channels presented in Fig. 4 and in the text, for methanol and its deuterated isotopologues, with uncertainties representing one standard deviation. The two electron regions are illustrated in Fig. 1. NM indicates a channel that was not measured.

Channel	CH_3OH	CH_3OD	CD_3OH
Parent ion	30 ± 3	43 ± 6	36 ± 6
e^- region 1	29 ± 2	39 ± 9	NM
Fragment ion	45 ± 4	91 ± 8	56 ± 6
e^- region 2	48 ± 4	97 ± 16	NM

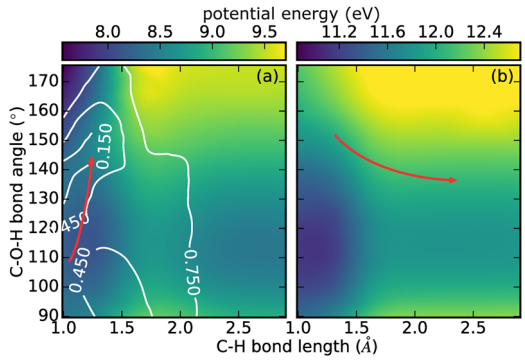

FIG. 5. 2-dimensional cuts of (a) the S_2 and S_3 excited state PES, where the lower of the two surfaces is illustrated by the color map (energy scale in eV) and the difference $|S_3 - S_2|$ by white contours, and (b) the cation ground state D_0 PES (energy scale in eV). The excited state wavepacket in the Franck-Condon region of S_3 experiences a potential favoring C–O–H angle opening, leading to a conical intersection between S_3 and S_2, as indicated by the red arrow in panel (a). A C–H dissociation path on the cation surface D_0, indicated by a red arrow in panel (b), may follow ionization of the excited neutral system by a single probe photon, for open C–O–H angles $\gtrsim 140°$ and pump-probe time delays between 10 fs and 200 fs.

the results of Buenker *et al.*[34] and the observed increase in decay time with hydroxyl deuteration, both of which showed this bond angle to play a key role. Other degrees of freedom were considered, for instance, a linear interpolation between reactants and products with orthogonal degrees optimized, and we determined the most relevant information to be in Fig. 5 (see the supplementary material for a discussion of the other degrees of freedom). The cuts reveal a path for a fraction of the cation wavepacket on D_0 to dissociate by C–H bond cleavage. The pathway is reached following ionization by the probe photon for C–O–H angles $\gtrsim 140°$, which are accessed through a conical intersection between the S_2 and S_3 states. A low potential energy barrier (<400 meV) on S_2 to angle opening is consistent with the delayed onset of the CH_2OH^+ fragment ion and the correlated lower-energy photoelectrons in the present measurements on CH_3OH. Such a barrier also provides a possible explanation for the longer CH_2OD^+ fragment ion and photoelectron decay times observed in the present measurements on deuterated methanol CH_3OD. Significant barriers around 1.7 Å on both of the S_2 and S_3 cuts may inhibit direct C–H dissociation by 156 nm photoexcitation, as observed in previous experimental investigations;[32] however, motion along other coordinates reduce the barriers.

IV. CONCLUSIONS

We have measured and described the ultrafast dynamics of methanol after 156 nm photoexcitation and demonstrated sensitivity to the coupled electronic and nuclear motion immediately following electronic excitation, using the analysis of onset and decay times in time-resolved photoelectron spectral features. By calculating cuts through the potential energy surfaces of the electronic excited states, we find mechanisms to explain the measured dissociation processes, invoking a previously unexplored A′ electronic state S_3. This state is accessed nonadiabatically through a conical intersection, and it dissociates rapidly along the C–O bond. The nonadiabatic transition from the photoexcited S_2 state to the dissociative S_3 state can occur within 15 fs of excitation. C–H dissociation was observed to be delayed relative to the C–O dissociation process and was determined to occur on the ground electronic state of the methanol cation, following significant C–O–H angle opening, facilitated by the conical intersection between the neutral states S_3 and S_2.

Comparison of the time-resolved measurements with the computed PES cuts enables the identification of the relevant reaction coordinates and a reduction in dimensionality of the dynamics. Resolving nuclear motion in higher dimensions through this procedure could be possible in further experiments involving photoionization to multiple electronic continua, given that the valence electron binding energies have unique dependencies on molecular configuration. These approaches could enable a more detailed understanding of nonadiabatic dynamics in electronically excited polyatomic molecules and may also be useful in studying highly coupled electronic nuclear motion, even on sub-10 fs time scales.[64,65]

SUPPLEMENTARY MATERIAL

See supplementary material for further details on the calculations of the potential energy surface cuts for the relevant electronic excited states of methanol and of the fitting procedure.

ACKNOWLEDGMENTS

This research used resources of the National Energy Research Scientific Computing Center, a United States Department of Energy (U.S. DOE) Office of Science User Facility supported by the Office of Science of the DOE, and was supported by the DOE, Office of Science, Office of Basic Energy Sciences, Chemical Sciences, Geosciences, and Biosciences Division, under Contract No. DE-AC02-05CH11231. Work at the University of California, Davis was supported by the U.S. Army Research Laboratory and the U.S. Army Research Office under Grant No. W911NF-14-1-0383.

REFERENCES

[1] A. H. Zewail, "Laser femtochemistry," Science **242**, 1645–1653 (1988).
[2] W. K. Peters, D. E. Couch, B. Mignolet, X. Shi, Q. L. Nguyen, R. C. Fortenberry, H. B. Schlegel, F. Remacle, H. C. Kapteyn, M. M. Murnane, and W. Li, "Ultrafast 25-fs relaxation in highly excited states of methyl azide mediated by strong nonadiabatic coupling," Proc. Natl. Acad. Sci. U. S. A. **114**, E11072–E11081 (2017).
[3] H. Timmers, Z. Li, N. Shivaram, R. Santra, O. Vendrell, and A. Sandhu, "Coherent electron hole dynamics near a conical intersection," Phys. Rev. Lett. **113**, 113003 (2014).
[4] M. C. E. Galbraith, S. Scheit, N. V. Golubev, G. Reitsma, N. Zhavoronkov, V. Despré, F. Lépine, A. I. Kuleff, M. J. J. Vrakking, O. Kornilov, H. Köppel, and J. Mikosch, "Few-femtosecond passage of conical intersections in the benzene cation," Nat. Commun. **8**, 1018 (2017).
[5] A. Ludwig, E. Liberatore, J. Herrmann, L. Kasmi, P. López-Tarifa, L. Gallmann, U. Rothlisberger, U. Keller, and M. Lucchini, "Ultrafast relaxation dynamics of the ethylene cation $C_2H_4^+$," J. Phys. Chem. Lett. **7**, 1901–1906 (2016).
[6] B. Joalland, T. Mori, T. J. Martínez, and A. G. Suits, "Photochemical dynamics of ethylene cation $C_2H_4^+$," J. Phys. Chem. Lett. **5**, 1467–1471 (2014).
[7] S. Adachi, T. Schatteburg, A. Humeniuk, R. Mitrić, and T. Suzuki, "Probing ultrafast dynamics during and after passing through conical intersections," Phys. Chem. Chem. Phys. (published online, 2019).

[8]D. R. Yarkony, "Diabolical conical intersections," Rev. Mod. Phys. **68**, 985–1013 (1996).
[9]B. G. Levine and T. J. Martínez, "Isomerization through conical intersections," Annu. Rev. Phys. Chem. **58**, 613–634 (2007).
[10]T. Ergler, A. Rudenko, B. Feuerstein, K. Zrost, C. D. Schröter, R. Moshammer, and J. Ullrich, "Spatiotemporal imaging of ultrafast molecular motion: Collapse and revival of the D_2^+ nuclear wave packet," Phys. Rev. Lett. **97**, 193001 (2006).
[11]Y. Nabekawa, Y. Furukawa, T. Okino, A. A. Eilanlou, E. J. Takahashi, K. Yamanouchi, and K. Midorikawa, "Sub-10-fs control of dissociation pathways in the hydrogen molecular ion with a few-pulse attosecond pulse train," Nat. Commun. **7**, 12835 (2016).
[12]P. Sándor, V. Tagliamonti, A. Zhao, T. Rozgonyi, M. Ruckenbauer, P. Marquetand, and T. Weinacht, "Strong field molecular ionization in the impulsive limit: Freezing vibrations with short pulses," Phys. Rev. Lett. **116**, 063002 (2016).
[13]M. C. E. Galbraith, C. T. L. Smeenk, G. Reitsma, A. Marciniak, V. Despré, J. Mikosch, N. Zhavoronkov, M. J. J. Vrakking, O. Kornilov, and F. Lépine, "XUV-induced reactions in benzene on sub-10 fs timescale: Nonadiabatic relaxation and proton migration," Phys. Chem. Chem. Phys. **19**, 19822–19828 (2017).
[14]A. Stolow, A. E. Bragg, and D. M. Neumark, "Femtosecond time-resolved photoelectron spectroscopy," Chem. Rev. **104**, 1719–1758 (2004).
[15]A. Stolow, "Femtosecond time-resolved photoelectron spectroscopy of polyatomic molecules," Annu. Rev. Phys. Chem. **54**, 89–119 (2003).
[16]D. M. Neumark, "Time-resolved photoelectron spectroscopy of molecules and clusters," Annu. Rev. Phys. Chem. **52**, 255–277 (2001).
[17]H. Satzger, D. Townsend, and A. Stolow, "Reassignment of the low lying cationic states in gas phase adenine and 9-methyl adenine," Chem. Phys. Lett. **430**, 144–148 (2006).
[18]C. Z. Bisgaard, O. J. Clarkin, G. Wu, A. M. D. Lee, O. Geßner, C. C. Hayden, and A. Stolow, "Time-resolved molecular frame dynamics of fixed-in-space CS_2 molecules," Science **323**, 1464–1468 (2009).
[19]P. Hockett, E. Ripani, A. Rytwinski, and A. Stolow, "Probing ultrafast dynamics with time-resolved multi-dimensional coincidence imaging: Butadiene," J. Mod. Opt. **60**, 1409–1425 (2013).
[20]H. Marciniak and S. Lochbrunner, "On the interpretation of decay associated spectra in the presence of time dependent spectral shifts," Chem. Phys. Lett. **609**, 184–188 (2014).
[21]M. H. Elkins, H. L. Williams, and D. M. Neumark, "Isotope effect on hydrated electron relaxation dynamics studied with time-resolved liquid jet photoelectron spectroscopy," J. Chem. Phys. **144**, 184503 (2016).
[22]Y.-I. Suzuki, T. Horio, T. Fuji, and T. Suzuki, "Time-resolved photoelectron imaging of S_2–S_1 internal conversion in benzene and toluene," J. Chem. Phys. **134**, 184313 (2011).
[23]T. Fuji, Y.-I. Suzuki, T. Horio, and T. Suzuki, "Excited-state dynamics of CS_2 studied by photoelectron imaging with a time resolution of 22 fs," Chem. - Asian J. **6**, 3028–3034 (2011).
[24]T. Horio, Y.-i. Suzuki, and T. Suzuki, "Ultrafast photodynamics of pyrazine in the vacuum ultraviolet region studied by time-resolved photoelectron imaging using 7.8-eV pulses," J. Chem. Phys. **145**, 044307 (2016).
[25]T. Kobayashi, T. Horio, and T. Suzuki, "Ultrafast deactivation of the $\pi\pi^*(V)$ state of ethylene studied using sub-20 fs time-resolved photoelectron imaging," J. Phys. Chem. A **119**, 9518–9523 (2015).
[26]E. G. Champenois, N. H. Shivaram, T. W. Wright, C.-S. Yang, A. Belkacem, and J. P. Cryan, "Involvement of a low-lying Rydberg state in the ultrafast relaxation dynamics of ethylene," J. Chem. Phys. **144**, 014303 (2016).
[27]T. Horio, R. Spesyvtsev, K. Nagashima, R. A. Ingle, Y.-i. Suzuki, and T. Suzuki, "Full observation of ultrafast cascaded radiationless transitions from $S_2(\pi\pi^*)$ state of pyrazine using vacuum ultraviolet photoelectron imaging," J. Chem. Phys. **145**, 044306 (2016).
[28]G. A. Olah, A. Goeppert, and G. K. S. Prakash, *Beyond Oil and Gas: The Methanol Economy* (Wiley VCH, Weinheim, 2009), oCLC: 587391600.
[29]G. A. Olah, "Beyond oil and gas: The methanol economy," Angew. Chem., Int. Ed. **44**, 2636–2639 (2005).
[30]J. Kothandaraman, A. Goeppert, M. Czaun, G. A. Olah, and G. K. S. Prakash, "Conversion of CO_2 from air into methanol using a polyamine and a homogeneous ruthenium catalyst," J. Am. Chem. Soc. **138**, 778–781 (2016).
[31]S. Harich, J. J. Lin, Y. T. Lee, and X. Yang, "Competing atomic and molecular hydrogen pathways in the photodissociation of methanol at 157 nm," J. Chem. Phys. **111**, 5–9 (1999).
[32]S. Harich, J. J. Lin, Y. T. Lee, and X. Yang, "Photodissociation dynamics of methanol at 157 nm," J. Phys. Chem. A **103**, 10324–10332 (1999).
[33]B.-M. Cheng, M. Bahou, W.-C. Chen, C.-h. Yui, Y.-P. Lee, and L. C. Lee, "Experimental and theoretical studies on vacuum ultraviolet absorption cross sections and photodissociation of CH_3OH, CH_3OD, CD_3OH, and CD_3OD," J. Chem. Phys. **117**, 1633–1640 (2002).
[34]R. J. Buenker, G. Olbrich, H. P. Schuchmann, B. L. Schuermann, and C. Von Sonntag, "Photolysis of methanol at 185 nm. Quantum-mechanical calculations and product study," J. Am. Chem. Soc. **106**, 4362–4368 (1984).
[35]K.-j. Yuan, Y. Cheng, F.-y. Wang, and X.-m. Yang, "Photodissociation dynamics of methanol and ethanol at 157 nm," Chin. J. Chem. Phys. **21**, 301 (2008).
[36]J. G. Philis, "Resonance-enhanced multiphoton ionization spectra of jet-cooled methanol and ethanol," Chem. Phys. Lett. **449**, 291–295 (2007).
[37]Z. Chen, A. T. J. B. Eppink, B. Jiang, G. C. Groenenboom, X. Yang, and D. H. Parker, "Product pair correlation in CH_3OH photodissociation at 157 nm: The OH + CH_3 channel," Phys. Chem. Chem. Phys. **13**, 2350–2355 (2011).
[38]J. G. Izquierdo, G. A. Amaral, F. Ausfelder, F. J. Aoiz, and L. Bañares, "Velocity map imaging study of the photodissociation of CH_3SH: Internal energy distribution of the SH fragment," ChemPhysChem **7**, 1682–1686 (2006).
[39]J. E. Stevens, H. W. Jang, L. J. Butler, and J. C. Light, "An adiabatic model for the photodissociation of CH_3SH in the first ultraviolet absorption band," J. Chem. Phys. **102**, 7059–7069 (1995).
[40]D. R. Yarkony, "On the role of conical intersections of two potential energy surfaces of the same symmetry in photodissociation. I. $CH_3SH \rightarrow CH_3S + H$ and CH_3 + SH," J. Chem. Phys. **100**, 3639–3644 (1994).
[41]N. Shivaram, E. G. Champenois, J. P. Cryan, T. Wright, T. Wingard, and A. Belkacem, "Focal overlap gating in velocity map imaging to achieve high signal-to-noise ratio in photo-ion pump-probe experiments," Appl. Phys. Lett. **109**, 254101 (2016).
[42]G. A. Garcia, L. Nahon, and I. Powis, "Two-dimensional charged particle image inversion using a polar basis function expansion," Rev. Sci. Instrum. **75**, 4989–4996 (2004).
[43]T. Korona and H.-J. Werner, "Local treatment of electron excitations in the EOM-CCSD method," J. Chem. Phys. **118**, 3006–3019 (2003).
[44]H. J. Monkhorst, "Calculation of properties with the coupled-cluster method," Int. J. Quantum Chem. **12**, 421–432 (1977).
[45]T. H. Dunning, "Gaussian basis sets for use in correlated molecular calculations. I. The atoms boron through neon and hydrogen," J. Chem. Phys. **90**, 1007–1023 (1989).
[46]P. J. Knowles, C. Hampel, and H.-J. Werner, "Coupled cluster theory for high spin, open shell reference wave functions," J. Chem. Phys. **99**, 5219–5227 (1993).
[47]P. J. Knowles, C. Hampel, and H.-J. Werner, "Erratum: 'Coupled cluster theory for high spin, open shell reference wave functions' [J. Chem. Phys. **99**, 5219 (1993)]," J. Chem. Phys. **112**, 3106–3107 (2000).
[48]M. Valiev, E. J. Bylaska, N. Govind, K. Kowalski, T. P. Straatsma, H. J. J. Van Dam, D. Wang, J. Nieplocha, E. Apra, T. L. Windus, and W. A. de Jong, "NWChem: A comprehensive and scalable open-source solution for large scale molecular simulations," Comput. Phys. Commun. **181**, 1477–1489 (2010).
[49]S. Hirata, "Symbolic algebra in quantum chemistry," Theor. Chem. Acc. **116**, 2–17 (2006).
[50]D. C. Comeau and R. J. Bartlett, "The equation-of-motion coupled-cluster method. Applications to open- and closed-shell reference states," Chem. Phys. Lett. **207**, 414–423 (1993).
[51]R. J. Bartlett and G. D. Purvis, "Many-body perturbation theory, coupled-pair many-electron theory, and the importance of quadruple excitations for the correlation problem," Int. J. Quantum Chem. **14**, 561–581 (1978).
[52]R. J. Bartlett and G. D. Purvis III, "Molecular applications of coupled cluster and many-body perturbation methods," Phys. Scr. **21**, 255 (1980).

[53]H.-J. Werner, P. J. Knowles, G. Knizia, F. R. Manby, M. Schütz, P. Celani, T. Korona, R. Lindh, A. Mitrushenkov, G. Rauhut, K. R. Shamasundar, T. B. Adler, R. D. Amos, A. Bernhardsson, A. Berning, D. L. Cooper, M. J. O. Deegan, A. J. Dobbyn, F. Eckert, E. Goll, C. Hampel, A. Hesselmann, G. Hetzer, T. Hrenar, G. Jansen, C. Köppl, Y. Liu, A. W. Lloyd, R. A. Mata, A. J. May, S. J. McNicholas, W. Meyer, M. E. Mura, A. Nicklass, D. P. O'Neill, P. Palmieri, D. Peng, K. Pflüger, R. Pitzer, M. Reiher, T. Shiozaki, H. Stoll, A. J. Stone, R. Tarroni, T. Thorsteinsson, and M. Wang, MOLPRO, version 2012.1, a package of *ab initio* programs, 2012, see http://www.molpro.net/.

[54]H.-J. Werner, P. J. Knowles, G. Knizia, F. R. Manby, and M. Schütz, "Molpro: A general-purpose quantum chemistry program package," Wiley Interdiscip. Rev.: Comput. Mol. Sci. **2**, 242–253 (2012).

[55]J. A. Nelder and R. Mead, "A simplex method for function minimization," Comput. J. **7**, 308–313 (1965).

[56]H.-J. Werner, "Third-order multireference perturbation theory the CASPT3 method," Mol. Phys. **89**, 645–661 (1996).

[57]P. Celani and H.-J. Werner, "Multireference perturbation theory for large restricted and selected active space reference wave functions," J. Chem. Phys. **112**, 5546–5557 (2000).

[58]H.-J. Werner and P. J. Knowles, "A second order multiconfiguration SCF procedure with optimum convergence," J. Chem. Phys. **82**, 5053–5063 (1985).

[59]P. J. Knowles and H.-J. Werner, "An efficient second-order MC SCF method for long configuration expansions," Chem. Phys. Lett. **115**, 259–267 (1985).

[60]K. A. G. Macneil and R. N. Dixon, "High-resolution photoelectron spectroscopy of methanol and its deuterated derivatives: Internal rotation in the ground ionic state," J. Electron Spectrosc. Relat. Phenom. **11**, 315–331 (1977).

[61]D. Townsend, H. Satzger, T. Ejdrup, A. M. D. Lee, H. Stapelfeldt, and A. Stolow, "$^1B_2(^1\Sigma_u^+)$ excited state decay dynamics in CS_2," J. Chem. Phys. **125**, 234302 (2006).

[62]C. C. Marston, K. Weide, R. Schinke, and H. U. Suter, "Product selectivity of vibrationally mediated photofragmentation of methanol," J. Chem. Phys. **98**, 4718–4727 (1993).

[63]J. Momigny, H. Wankenne, and C. Krier, "Correlation diagram approach to the dissociative ionization mechanisms of methanol," Int. J. Mass Spectrom. Ion Phys. **35**, 151–170 (1980).

[64]F. Calegari, D. Ayuso, A. Trabattoni, L. Belshaw, S. D. Camillis, S. Anumula, F. Frassetto, L. Poletto, A. Palacios, P. Decleva, J. B. Greenwood, F. Martín, and M. Nisoli, "Ultrafast electron dynamics in phenylalanine initiated by attosecond pulses," Science **346**, 336–339 (2014).

[65]M. Vacher, M. J. Bearpark, M. A. Robb, and J. P. Malhado, "Electron dynamics upon ionization of polyatomic molecules: Coupling to quantum nuclear motion and decoherence," Phys. Rev. Lett. **118**, 083001 (2017).